Cancer Chemother Pharmacol (2011) 68:923–933
DOI 10.1007/s00280-011-1568-1

ORIGINAL ARTICLE

SCH 1473759, a novel Aurora inhibitor, demonstrates enhanced anti-tumor activity in combination with taxanes and KSP inhibitors

Andrea D. Basso · Ming Liu · Kimberly Gray · Seema Tevar · Suining Lee · Lianzhu Liang · Abdul Ponery · Elizabeth B. Smith · Frederick J. Monsma Jr. · Tao Yu · Yonglian Zhang · Angela D. Kerekes · Sara Esposite · Yushi Xiao · Jayaram R. Tagat · Daniel J. Hicklin · Paul Kirschmeier

Received: 13 October 2010 / Accepted: 17 January 2011 / Published online: 5 February 2011

Abstract
Purpose Aurora kinases are required for orderly progression of cells through mitosis, and inhibition of these kinases by siRNA or small molecule inhibitors results in cell death. We previously reported the synthesis of SCH 1473759, a novel sub-nanomolar Aurora A/B inhibitor.
Methods We utilized SCH 1473759 and a panel of tumor cell lines and xenograft models to gain knowledge about optimal dosing schedule and chemotherapeutic combinations for Aurora A/B inhibitors.
Results SCH 1473759 was active against a large panel of tumor cell lines from different tissue origin and genetic backgrounds. Asynchronous cells required 24-h exposure to SCH 1473759 for maximal induction of >4 N DNA content and inhibition of cell growth. However, following taxane- or KSP inhibitor-induced mitotic arrest, less than 4-h exposure induced >4 N DNA content. This finding correlated with the ability of SCH 1473759 to accelerate exit from mitosis in response to taxane- and KSP inhibitor-induced arrest. We tested various dosing schedules in vivo and demonstrated SCH 1473759 dose- and schedule-dependent anti-tumor activity in four human tumor xenograft models. Further, the efficacy was enhanced in combination with taxanes and found to be most efficacious when SCH 1473759 was dosed 12-h post-taxane treatment.
Conclusions SCH 1473759 demonstrated potent mechanism-based activity, and activity was shown to be enhanced in combination with taxanes and KSP inhibitors. This information may be useful for optimizing the clinical efficacy of Aurora inhibitors.

Keywords Aurora · Taxane · KSP

Abbreviations

HPBCD	Hydroxypropyl B cyclodextrin
IHC	Immunohistochemistry
i.p.	Intraperitoneal
TGI	Tumor growth inhibition
twice daily	bid
daily	qd
weekly	q7d

Introduction

Aurora kinases (Aurora A, B, C) are cell cycle-regulated serine/threonine kinases that play a role in regulating mitosis. Aurora A and B kinases are frequently overexpressed in a wide range of human cancers and in some cases, over

Electronic supplementary material The online version of this article (doi:10.1007/s00280-011-1568-1) contains supplementary material, which is available to authorized users.

A. D. Basso · M. Liu · K. Gray · S. Tevar · S. Lee · L. Liang · A. Ponery · D. J. Hicklin · P. Kirschmeier
Department of Oncology, Merck Research Laboratories, 2015 Galloping Hill Road, Kenilworth, NJ 07033, USA

E. B. Smith · F. J. Monsma Jr.
Department of Discovery Technologies, Merck Research Laboratories, 2015 Galloping Hill Road, Kenilworth, NJ 07033, USA

T. Yu · Y. Zhang · A. D. Kerekes · S. Esposite · Y. Xiao · J. R. Tagat
Department of Chemistry, Merck Research Laboratories, 2015 Galloping Hill Road, Kenilworth, NJ 07033, USA

A. D. Basso (✉)
2015 Galloping Hill Rd, Kenilworth, NJ 07093, USA
e-mail: andrea.basso@merck.com

expression correlates with allelic imbalance, higher clinical grade, tumor invasiveness, and poor prognosis [1]. Aurora A regulates centrosome maturation and microtubule nucleation. Aurora A also phosphorylates proteins required for bipolar spindle assembly and mitotic entry. Aurora B along with three nonenzymatic subunits (INCENP, survivin, and borealin/dasra) make up the chromosome passenger complex, which regulates chromatin remodeling, kinetochore-spindle attachment, and cytokinesis [2, 3]. Aurora B regulates chromatin structure in part by phosphorylating proteins including Histone H3 [4, 5]. In its role in kinetochore-spindle attachment, Aurora B monitors biorientation and tension [6]. In so doing, Aurora B fixes incorrect spindle attachments by weakening the attachment and allowing for the establishment of new correct attachments [7]. Aurora B regulates cytokinesis via phosphorylation of intermediate filaments and RhoA/Rac-GAP [2]. Aurora C functions similarly to Aurora B but is mainly expressed in testis and plays a role during spermatogenesis [8, 9].

Depletion of Aurora A alone by siRNA results in lagging chromosomes and mitotic defects, while ablation of Aurora B results in chromosome misalignment at metaphase, unequal chromosome segregation at anaphase, followed by a failure to undergo cytokinesis and premature mitotic exit resulting in polyploidy (contains >4 N DNA content) and cell death. Combined depletion of Aurora A and B by siRNA results in polyploid cells, a phenotype identical to that induced by ablation of Aurora B alone [10]. Aurora B function is apparently required for the checkpoint induced by loss of Aurora A. Importantly, inhibition of Aurora A does not interfere with the phenotypic consequences of Aurora B inhibition.

Inhibition of Aurora kinases results in disruption of cell division and induction of cell death. Thus, disruption of normal Aurora function is expected to impair tumor growth and thereby has potential for activity in a number of human cancers. Several small molecule dual inhibitors of Aurora A and B kinases have been synthesized including MK-0457 and AT-9283 and demonstrate anti-tumor activity in preclinical models [11, 12]. Additionally, selective Aurora A (e.g. MLN8054) and selective Aurora B (e.g. AZD-1152) have also demonstrated activity in preclinical models [13, 14]. Aurora kinase inhibitors have entered the clinic, and their activity is being explored in solid tumors and hematological diseases [15].

We have identified a novel sub-nanomolar Aurora A/B inhibitor, SCH 1473759, which demonstrates potent mechanism-based cell activity. We found that 24-h exposure to SCH 1473759 was required for optimal biological effect in tumor cell lines. However, following a taxane or KSP inhibitor mitotic arrest, less than 4-h exposure was sufficient to induce >4 N DNA content. This finding correlated with the ability of SCH 1473759 to accelerate exit from mitosis in response to taxane- and KSP inhibitor-induced arrest. We tested various dosing schedules in vivo and demonstrated SCH 1473759 was efficacious in four human tumor xenograft models and demonstrated enhanced activity with taxanes. Further, we found the combination to be most effective when SCH 1473759 was dosed 12 h post-taxane treatment.

Materials and methods

Materials

For in vitro studies, SCH 1473759 and SB-715992 (synthesized at Schering-Plough [16]) and docetaxel (Sigma) were dissolved in DMSO and ethanol, respectively. For in vivo studies, SCH 1473759 and paclitaxel (Bristol-Myers Squibb Company) were dissolved in 20% hydroxypropyl B cyclodextrin (HPBCD).

Cell culture

Human tumor cell lines were grown in DMEM:F12 media supplemented with 2 mM glutamine, 50 units/ml penicillin, 50 units/ml streptomycin with 10% heat inactivated fetal bovine serum (Invitrogen) at 37°C with 5% CO_2. Cells were obtained from ATCC, with the exception of SNB19, SNB87, U251 (NCI tumor repository) and A2780 (kindly provided by Dr. Janet Price, M.D. Anderson).

Immunofluorescent assays

HCT-116 cells were plated at 15,000 cells per well in poly-D-lysine coated black micro-clear 384-well tissue culture plates. For the phos-Histone H3 assay, cells were first treated with 0.4 μg/ml nocodazole for 16 h. Subsequently, cells were treated for 1 h with compound (0.1% final DMSO concentration) in triplicate wells. Cells were fixed with Prefer® fixation solution (Anatech) plus 1,000 nM Hoechst 33342 dye and incubated for 30 min at room temperature. The fixation solution was removed, and cells were washed with PBS. Cells were permeabilized with 0.2% Triton-X in PBS and incubated for 10 min. Cells were washed with PBS and incubated with PBS containing 3% FBS for 30 min. Cells were then stained overnight at 4°C with Phos-Histone H3 (ser10)-Alexa Fluor 488 Conjugate antibody (Cell Signaling) solution in PBS plus 3% FBS. Cells were washed with PBS, and then immunofluorescence images were captured at 10× using the HT Pathway 855 automated fluorescent microscope (BD Bioscience). Percent positive cells were quantitated by Hoechst staining for total cell number using Attovision software (BD Bioscience). To generate IC50 values, the dose–response curves

were then fitted to a standard sigmoidal curve and IC50 values were derived by nonlinear regression analysis. For MPM-2 staining, 6 h after cell plating the media was removed and cells were treated for the indicated times with compound. The above staining protocol was followed using Phos-MPM2-Texas Red Conjugate (Millipore).

Cell cycle analysis

HCT-116 cells were plated using 2×10^6 cells per 10-cm tissue culture dish. The next day, cells were treated with compound (0.1% final DMSO concentration) and 24 h later collected and centrifuged for 1 min at 1,000 rpm. Cell pellet was resuspended in 0.5 ml PBS, and the solution was transferred to cold 70% methanol and incubated at −20°C for 30 min. Cells were then centrifuged for 1 min at 1,000 rpm, the supernatant was removed, pellet washed with 2 ml PBS, centrifuged, and supernatant removed. Cells were resuspended in 0.5 ml propidium iodine stain (0.1 mM EDTA, 0.05 mg/ml RNase, 50 ug/ml propidium iodine), transferred to a filter cap tube, and read by fluorescence-activated cell sorting (FACS).

Cell growth

Cells were plated at a cell density ranging from 625 to 3,750 cells per well depending on the rate of cell growth in poly-D-lysine coated black micro-clear 384-well tissue culture plates. Cells were treated in triplicate wells with compound (0.1% final DMSO concentration). A plate was stained at the start of the study (zero hour), and a second plate was incubated for 72 h at 37°C and then stained. Cells were fixed with Prefer® fixation solution plus 1,000 nM Hoechst 33342 dye and incubated for 30 min. The fixation solution was removed, and cells were washed twice with PBS. Then, immunofluorescence images were captured at 10× using the HT Pathway 855 automated fluorescent microscope. The difference in cell number between zero and 72 h was plotted against compound concentration, and the dose–response curves were fitted to a standard sigmoidal curve and IC50 values were derived by nonlinear regression analysis.

Immunohistochemistry (IHC)

Nu/nu mice (female, 5–7 weeks of age) were injected subcutaneously with 5×10^6 of A2780 cells/mouse. When tumor cells reached approximately 200–500 mm^3, mice were randomly grouped into treatment groups ($n = 3$). Animals were dosed through intraperitoneal injections. Tumors were excised from the animals, and the tissue was fixed in 10% buffered formaldehyde for 24 h and then trimmed to equal size (~ 75 mm^3) and processed for paraffin embedding using 30-min cycle on VIP tissue processing unit. Processed tissues were embedded in paraffin using in-lab developed tissue array method. Five-micrometer-thick sections were cut on microtome and mounted onto slides, which were then incubated overnight in 56°C oven and stained with phos-Histone H3 antibody (Millipore). IHC assays were performed using peroxidase-based polymer- IHC detection system (Dako Envision+ kit). Ten consecutive fields of positive area were imaged at 40× for analysis from each tumor sample. Image-Pro image analysis program was used for analysis.

Xenograft studies

Nu/nu mice (5–7 weeks of age) were injected subcutaneously with 5×10^6 cells/mouse. Female mice were used for A2780 and PA1, and male mice for 22RV-1 and DU-145 models. When tumor cells reached approximately 200 mm^3, mice were randomly grouped into treatment groups ($n = 10$). Tumor volumes and body weights were measured twice a week throughout the study using calipers and calculated by the formula (width × length × height) × $6/\pi$. Statistically significant differences were determined by the multiple comparison one-way ANOVA (Turkey's test) at the 95% confidence level using GraphPad Prism. All animal studies were carried out in accordance with institutional guidelines and the *NIH Guide for the Care and Use of Laboratory Animals.*

Results

Mechanism-based activity of SCH 1473759

We previously described the biochemical characterization of SCH 1473759, a potent sub-nanomolar inhibitor of Aurora A and B with Kd values of 0.02 and 0.03 nM, respectively [16]. Reported kinase counter screens have demonstrated that this compound has additional activities and also inhibits the Src family (IC50 < 10 nM), Chk1 (IC50 = 13 nM), VEGFR2 (IC50 = 1 nM), and IRAK4 (IC50 = 37 nM).

Inhibition of Aurora B activity in cells was measured by evaluating the phosphorylation of Histone H3 (serine-10), a direct downstream substrate of Aurora B [4, 5]. In order to increase the signal-to-noise ratio of the assay, HCT-116 cells were arrested in mitosis with nocodazole and 16 h later treated with increasing concentrations of SCH 1473759 for 1 h. Phosphorylation of Histone H3 was measured by immunofluorescence, and percent positive cells were quantified. SCH 1473759 was found to cause a dose-dependent decrease in the levels of phosphorylated Histone H3 with an IC50 value of 25 nM (Fig. 1a).

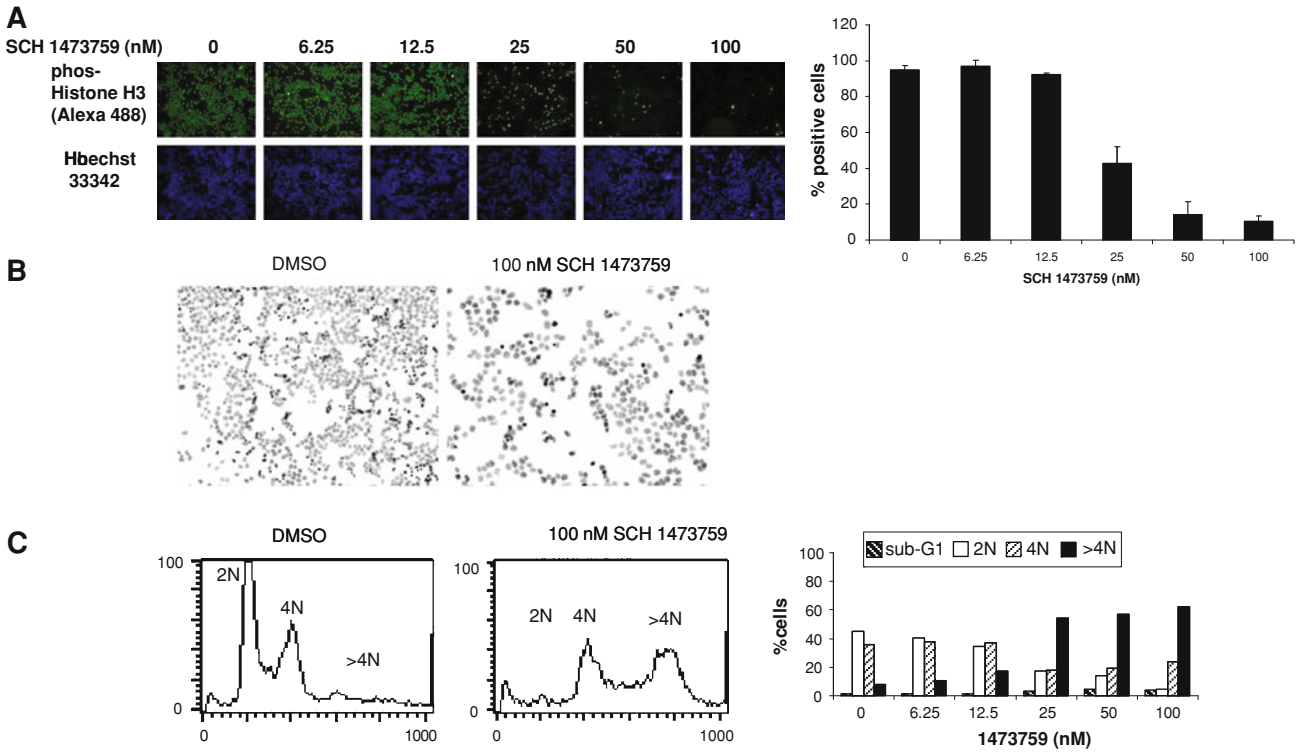

Fig. 1 SCH 1473759 treatment inhibited Histone H3 phosphorylation and resulted in cells with visually larger nuclei and >4 N DNA content. **a** HCT-116 cells were treated with nocodazole for 16 h followed by increasing concentrations of SCH 1473759 for 1 h. Histone H3 phosphorylation was detected by immunofluorescence and percent positive cells was quantified. **b** HCT-116 cells were treated with DMSO or 100 nM SCH 1473759 for 24 h and stained with Hoechst 33342. **c** HCT-116 cells were treated with increasing concentrations of SCH 1473759 for 24 h and DNA content was measured by FACS

Inhibition of Aurora B prevents cells from undergoing cytokinesis and leads to polyploid cells characterized by cells with >4 N DNA content [10]. Consistent with this phenotype, SCH 1473759-treated cells have larger nuclei as visualized by microscopy (Fig. 1b). To assess this phenotype further, asynchronous HCT-116 cells were treated with SCH 1473759 for 24 h and FACS was used to measure DNA content. Concentrations of SCH 1473759 over 25 nM resulted in cells with >4 N DNA content (Fig. 1c). This dose level resulted in 54% of cells with >4 N DNA content.

In order to assess the anti-proliferative effect of SCH 1473759, a panel of 53 tumor cell lines from different tissues (breast, ovarian, prostate, lung, colon, brain, gastric, renal, skin, and leukemia) was treated with the compound, and growth inhibition was measured 72 h later. SCH 1473759 inhibited 51/53 tumor cell lines with an IC50 values <100 nM (Supplementary Table 1). The mean IC50 value for tumor growth inhibition across this panel was 21 nM. The most sensitive cell lines included A2780, LNCap, N87, Molt4, K562, and CCRF-CEM with IC50 values <5 nM. SCH 1473759 failed to inhibit the growth of H23 and ASPC1 cells in the dose range tested. Additionally, we found 100 nM SCH 1473759 induced >4 N DNA content in each of the 51 cell lines growth inhibited (Supplementary Table 1).

Sensitivity of cells to SCH 1473759 appeared independent of known mutational status (e.g. p53), mRNA expression of Aurora A or B, and Aurora SNP status (data not shown).

Twenty-four-hour exposure to SCH 1473759 was required for optimal activity

HCT-116 cells were treated with SCH 1473759 for various lengths of time to determine the time required to optimally induce endoreduplication and inhibit cell growth. Cells were exposed to 25 nM SCH 1473759 for 4, 8, 12, or 24 h, compound was washed out, and cells were harvested for analysis by FACS at the end of 24 h (Fig. 2a). Exposure times of 4 h were insufficient for induction of >4 N DNA content, while 8–12-h exposure induced significant but sub-maximal levels of cells with >4 N DNA content (23–33%). Exposures times of 24 h induced significant amount of cells with >4 N DNA content (55%).

Exposure times of 24 h were also required for optimal cell growth inhibition, and exposure times less than that resulted in sub-optimal cell growth inhibition. HCT-116

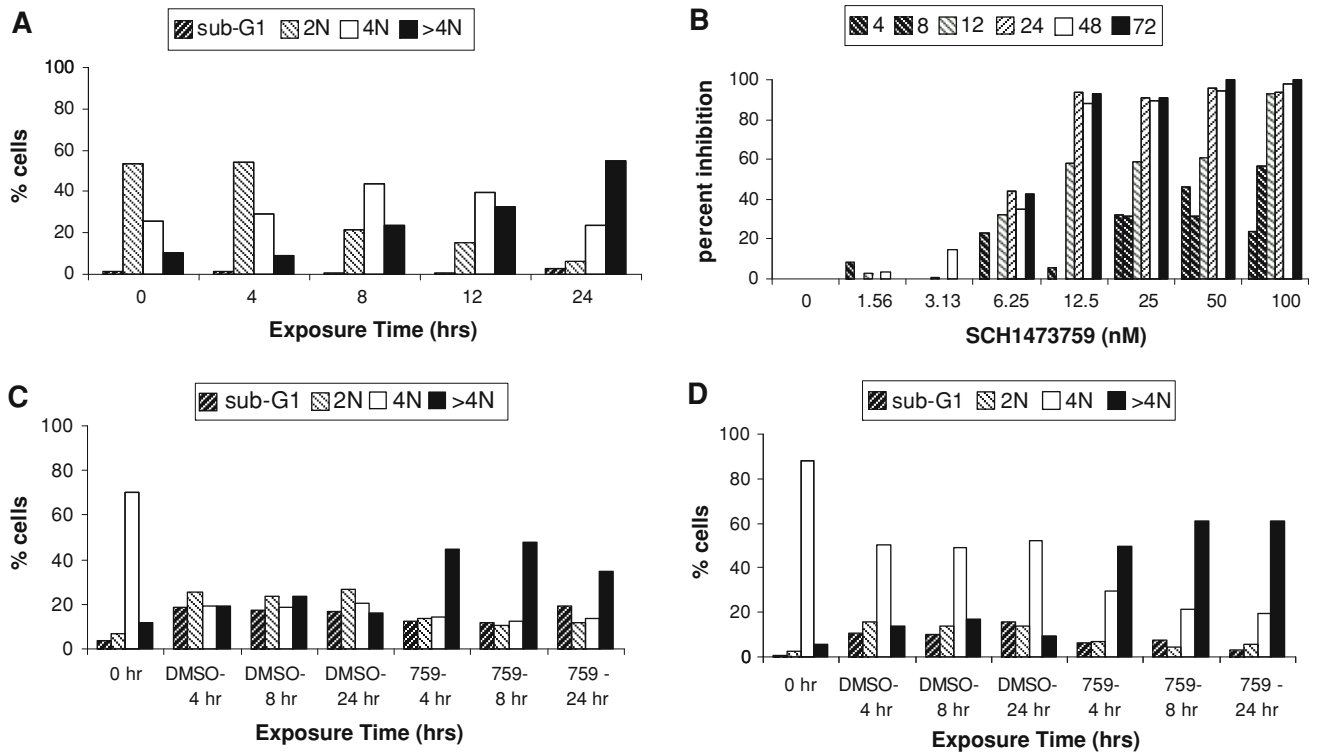

Fig. 2 Short exposure to SCH 1473759 was sufficient to induce >4 N DNA content following docetaxel- or KSP inhibitor-induced mitotic arrest. **a** HCT-116 cells were treated for the indicated times with 25 nM SCH 1473759 at which time compound was washed off and medium changed. DNA content was measured at the end of 24 h by FACS. **b** HCT-116 cells were treated for the indicated times with increasing concentrations of SCH 1473759 at which time the compound was washed off and the medium changed. Cell number was measured at the end of 72 h. **c**, **d** HCT-116 cells were treated with 5 nM docetaxel or 10 nM KSP inhibitor (SB-715992) for 16 h and then exposed to DMSO or 25 nM SCH 1473759 for 4, 8, and 24 h at which time the medium was changed. Cells were harvested at the end of 24 h and analyzed by FACS

cells were exposed to SCH 1473759 for various exposure times, followed by compound wash out. Cell growth inhibition was measured at the end of 72 h. Exposure for longer than 24 h to concentrations ≥12.5 nM SCH 1473759 inhibited cell growth by 90%. In contrast, 100 nM was required to achieve 90% growth inhibition using a 12-h exposure. Exposures for 4 or 8 h had significantly less effect on cell growth, and at these exposure times 12.5 nM failed to show any inhibition of cell growth (Fig. 2b).

Similar time-dependent exposure requirement for optimal induction of >4 N DNA content and cell growth inhibition was observed with structurally unrelated dual Aurora A/B inhibitors (250 nM MK-0457 and 100 nM AT-9283) and an Aurora B selective inhibitor (100 nM AZD-1152) (data not shown).

Short exposure to SCH 1473759 was sufficient to induce >4 N DNA content following taxane- or KSP inhibitor-induced mitotic arrest

Aurora kinase inhibitors act in mitosis when Aurora A and B are expressed; therefore, we hypothesized that combinations with anti-mitotic agents would increase the percentage of cells that could be targeted by an Aurora kinase inhibitor. By arresting cells in mitosis, docetaxel, paclitaxel, and KSP inhibitors increased the percentage of cells that are positive for Histone H3 and MPM2 phosphorylation. The percentage of positive cells was maximal 12–16 h post-treatment in vitro and in vivo (data not shown). We studied the combination of SCH 1473759 and taxanes or KSP inhibitors by treating cells with the anti-mitotic agent and dosing SCH 1473759 16 h later. HCT-116 colon cancer cells were treated with DMSO (data not shown), 5 nM docetaxel (Fig. 2c), or 10 nM KSP inhibitor (SB-715992) (Fig. 2d) for 16 h. Cells were then released into DMSO or 25 nM SCH 1473759-containing medium for the indicated times, at which point compound was washed out. All cells were evaluated for DNA content by FACS analysis at the end of 24 h. Following a 16-h pre-treatment with docetaxel or the KSP inhibitor, the time of exposure required for an Aurora kinase inhibitor to induce significant levels of >4 N DNA content was reduced and could be observed at 4 h (Fig. 2c, d).

To further explore the combination with anti-mitotics, we analyzed simultaneous treatment with an Aurora inhibitor. When cells were exposed to docetaxel or the KSP

inhibitor and SCH 1473759 concurrently, 4-h exposure did not induce significant levels of >4 N DNA content; significant levels were only observed after a 24-h exposure (Supplemental Fig. 1).

We also found pretreatment with docetaxel or a KSP inhibitor also reduced the time requirement for optimal induction of >4 N DNA content by structurally unrelated dual Aurora A/B inhibitors (250 nM MK-0457 and 100 nM AT-9283) and an Aurora B selective inhibitor (100 nM AZD-1152) (data not shown).

SCH 1473759 accelerated release from taxane- and KSP inhibitor-induced mitotic arrest

To further explore this combination, we examined the kinetics of mitotic exit by following the reduction of MPM2 phosphorylation, a marker of mitosis. We found that SCH 1473759 accelerated the exit from taxane- or KSP inhibitor-induced mitotic arrest (Fig. 3). HCT-116 colon cancer cells were pretreated with docetaxel or KSP inhibitor and then released into DMSO or SCH 1473759-containing medium. Cells released into DMSO medium maintained a high level of staining for MPM2 phosphorylation for up to 4 h. In HCT-116 cells, we found that increasing concentration of SCH 1473759 accelerated mitotic exit from docetaxel and KSP inhibitors, and by 4 h after compound treatment, most cells were negative for MPM2 phosphorylation (Fig. 3a, b).

To further explore this finding, we evaluated A2780 ovarian and 22RV-1 prostate tumor cells. SCH 1473759 accelerated mitotic exit from paclitaxel-induced arrest in A2780 (Fig. 3c) and docetaxel-induced arrest in 22RV-1 (Fig. 3d). Further, the accelerated mitotic exit by SCH 1473759 was observed from KSP inhibitor-induced arrest in both of these cell lines (data not shown).

Similar effects were seen with structurally unrelated dual Aurora A/B inhibitors (250 nM MK-0457 and 100 nM AT-9283), as well as with the Aurora B selective inhibitor 100 nM AZD-1152 (data not shown).

Pharmacodynamic effects of SCH 1473759

The pharmacodynamic marker, phosphorylation of Histone H3, was used to profile SCH 1473759 in vivo. This was assessed by intraperitoneal (*i.p.*) dosing of mice bearing A2780 ovarian tumor xenografts. Pharmacodynamic effects were not only assessed for single agent activity, but were also analyzed in combination with paclitaxel.

As a single agent, SCH 1473759 inhibited phosphorylation of Histone H3 in a dose-dependent manner (Fig. 4). One hour after treatment, increasing dose levels of SCH 1473759 (2.5, 10, 50, and 100 mg/kg) induced increasing

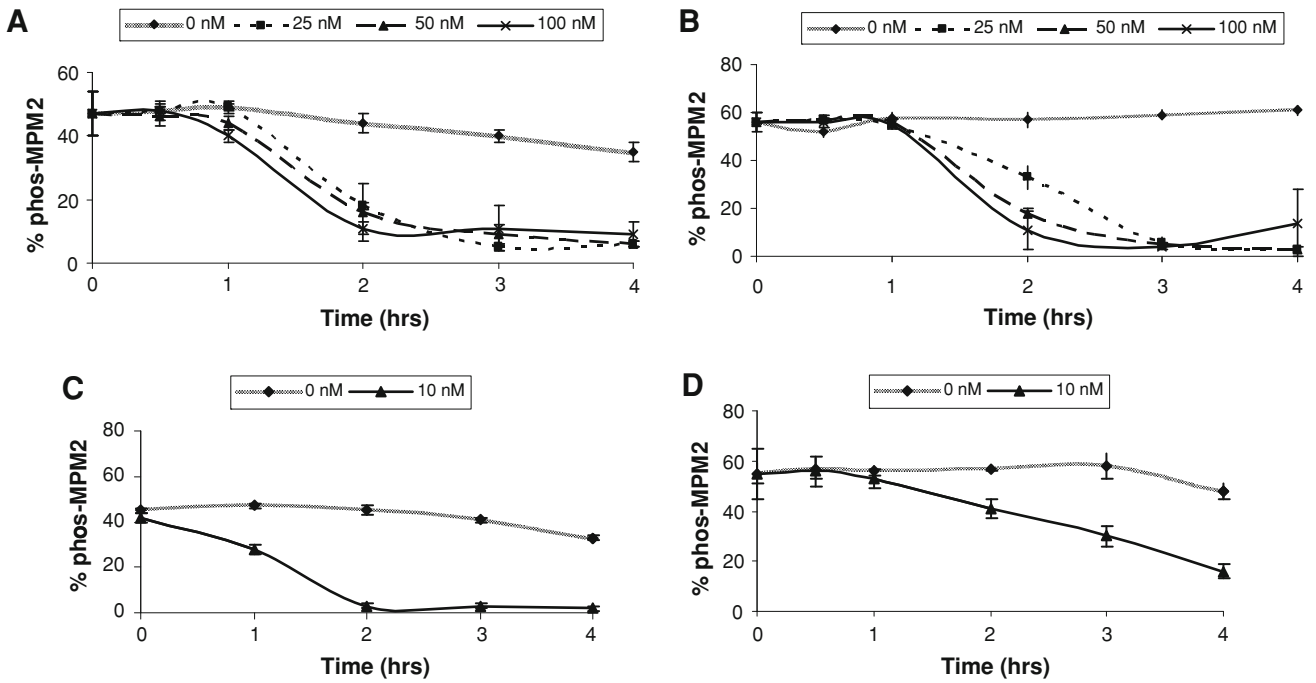

Fig. 3 SCH 1473759 accelerated release from docetaxel- and KSP inhibitor-induced mitotic arrest. **a** HCT-116 cells treated with 5 nM docetaxel or **b** 10 nM KSP inhibitor (SB-715992) for 16 h. **c** A2780 cells were treated with 50 nM docetaxel. **d** 22RV-1 cells were treated with 50 nM docetaxel. Cells were then released in DMSO, 10, 25, 50, or 100 nM SCH 1473759. Kinetic release from mitosis was measured by following phos-MPM2 by immunofluorescence

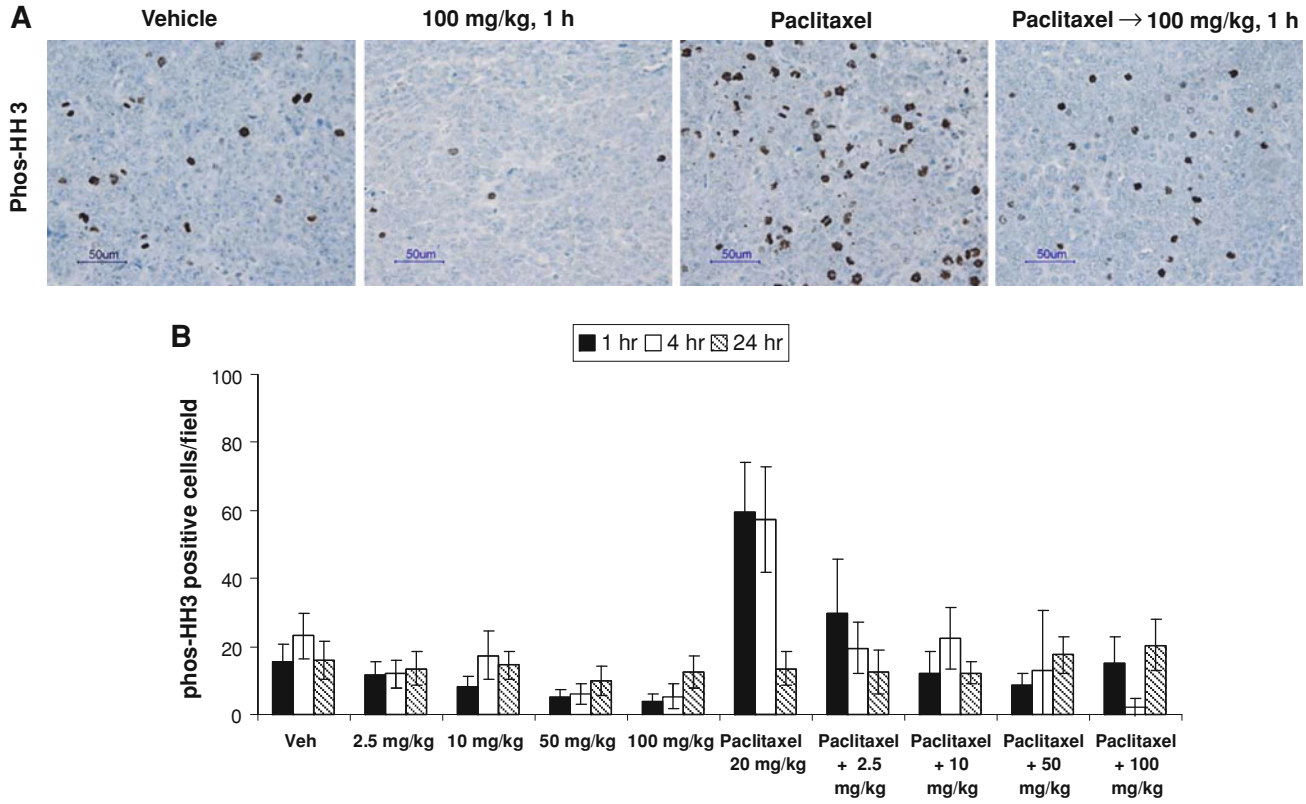

Fig. 4 SCH 1473759 inhibited basal- and paclitaxel-induced phos-Histone H3 in A2780 xenograft tumors. Mice bearing A2780 ovarian xenografts were dosed (*i.p.*) with vehicle or increasing doses of SCH 1473759. Additionally, animals previously dosed with 20 mg/kg paclitaxel 12 h earlier were dosed with vehicle or increasing doses of SCH 1473759. Tumors were collected at 1, 4, and 24 h after SCH 1473759 dose. Tumors were fixed and analyzed by IHC for phos-Histone H3

inhibition of the biomarker (31, 50, 69, and 75%, respectively). A similar pattern of dose-dependent inhibition remained at 4 h after treatment (48, 26, 74, and 78%). Histone H3 phosphorylation returned to basal levels 24 h after administration of SCH 1473759. The lack of sustained inhibition of the pharmacodynamic marker at 24 h post-treatment correlated with the short half-life for SCH 1473759 in the mouse, previously reported as 1 h [16].

Phosphorylation of Histone H3 was induced by paclitaxel, and maximal increase in this pharmacodynamic effect in tumors occurred 12–16 h after dosing (data not shown). Therefore, we evaluated the ability of SCH 1473759 to inhibit this induction, by first dosing mice with paclitaxel (20 mg/kg *i.p.*) followed by vehicle or SCH 1473759 12 h later. Paclitaxel treatment induced phosphorylation of Histone H3 fourfold compared to basal levels. This induction was not sustained over time and returned to basal levels 24 h later (Fig. 4). Administration of SCH 1473759 suppressed paclitaxel-induced phosphorylation of Histone H3 in a dose-dependent fashion. One hour after a single dose, increasing doses of SCH 1473759 (2.5, 10, 50, and 100 mg/kg) resulted in increasing inhibition of the pharmacodynamic marker (50, 80, 87, and 75%, respectively). This pattern of inhibition remained at 4 h after treatment (65, 61, 77, and 96%).

Plasma was collected from the mice at the same time the tumors were harvested, and the plasma level of SCH 1473759 was determined. Plasma concentrations increased with increasing dose and were highest 1 h post-dose, with concentrations at 24 h back to zero (data not shown). One hour following a 2.5 mg/kg dose, taxane-induced phosphorylation of Histone H3 was inhibited by 50%. At this time point, the plasma concentration of SCH 1473759 was 140 nM.

Efficacy of SCH 1473759 in human tumor xenografts

Initially, anti-tumor efficacy of SCH 1473759 dosed *i.p.* was evaluated in mice bearing established A2780 ovarian tumor xenografts. Three schedules were tested at their respective maximum tolerated doses: 10 mg/kg bid (twice daily), 20 mg/kg qd (daily), and 100 mg/kg day 0, 4, 7. Additionally, 60 mg/kg day 0, 4, 7 was tested. All four treatment schedules resulted in statistically significant tumor growth inhibition (TGI) compared to vehicle control. Tumor growth inhibition was dose- and schedule-dependent

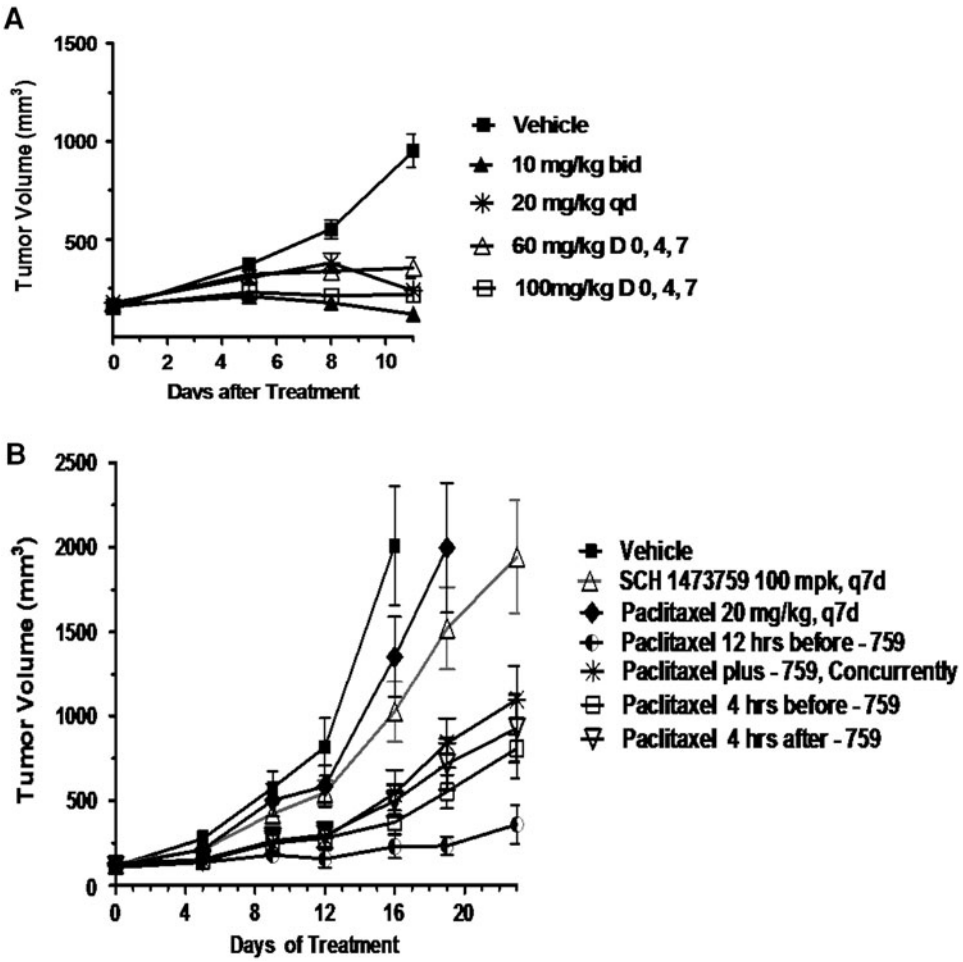

Fig. 5 SCH 1473759 demonstrated anti-tumor activity in A2780 ovarian tumor xenografts and enhanced paclitaxel efficacy. Mice bearing A2780 xenograft tumors were dosed with vehicle, SCH 1473759 (*i.p.*), paclitaxel (*i.p.*) or the combination at the indicated doses and schedules. Tumor volume was measured throughout the study

with SCH 1473759 bid dosing regimens resulting in better anti-tumor activity (106% TGI, 29% regressions) than qd (93% TGI) or intermittent schedules (73–93% TGI) at day 11 (Fig. 5a).

A second study was conducted to test weekly dosing (q7d) of SCH 1473759 in the A2780 ovarian tumor xenograft model. On this schedule, the maximally tolerated dose was determined to be 100 mg/kg. SCH 1473759 dosed at 100 mg/kg on a weekly schedule resulted in modest inhibition (52% TGI) of A2780 xenograft growth (Table 1).

To further explore whether continuous dosing was better than intermittent higher dosing, we treated mice bearing A2780 ovarian tumor xenografts with 20 mg/kg twice daily on days 0–4 and 15–18 or 40 mg/kg daily on days 0–4 and 15–18. Dosing breaks were designed in order to allow tolerance of higher doses. Similar to the initial study above, twice daily dosing was more efficacious (97 vs. 87% TGI) (Table 1).

The anti-tumor activity of SCH 1473759 was evaluated in three additional tumor xenograft models, including PA1 ovarian tumor and 22RV-1 and DU-145 prostate tumors (Table 1). Dosing on a q4d schedule with 100 mg/kg resulted in significant tumor growth inhibition in each of the three models: 81% in 22RV-1, 83% in DU-145, and 44% in PA1. Dosing below the maximally tolerated dose (60 mg/kg) on this schedule in mice bearing 22RV-1 tumor xenografts resulted in 51% TGI. We also tested weekly dosing (100 mg/kg) in 22RV-1 tumor xenografts models, where SCH 1473759 resulted in 61% TGI.

We further explored continuous dosing in mice bearing 22RV-1 tumors. Surprisingly, treatment resulted in significant body weight loss after 7 days. Toxicity observed at these dose levels was unexpected based on studies in female nude mice. These findings suggest that male nude mice are more sensitive to SCH 1473759. Additional studies using modified dosing schedule for male mice were used in subsequent studies (Table 1). Therefore, male mice bearing 22RV-1 tumor xenografts were dosed twice daily until body weight loss was observed (day 7), upon recovery of body weight (day 18) twice daily dosing was resumed. On this schedule, 5 and 10 mg/kg resulted in 51 and 87% TGI, respectively. Similarly, male mice bearing DU-145 tumor xenografts were dosed twice daily until body weight loss was observed and then dosing resumed upon recovery

Table 1 SCH 1473759 efficacy in xenograft models

Model	Dose (mg/kg)	Schedule	TGI (%)	*P* value
A2780	10	bid	106	<0.05
	20	qd	93	<0.05
	60	d0, 4, 7	73	<0.05
	100	d0, 4, 7	93	<0.05
A2780	100	q7d	52	>0.05
A2780	20	bid, d0-4, 15–18	97	<0.05
	40	qd, d0-4, 15–18	87	<0.05
22RV-1	60	q4d	51	<0.05
	100	q4d	81	<0.05
	100	q7d	61	<0.05
	5	bid, d0-7, 18–23	51	<0.05
	10	bid, d0-7, 18–23	87	<0.05
DU-145	7.5	bid, d0-10, 17–23	69	<0.01
	100	q4d	83	<0.05
PA-1	7.5	bid	78	<0.05
	100	q4d	44	<0.05

Mice bearing xenograft tumors were dosed with vehicle or SCH 1473759 (*i.p.*) at the indicated schedule and tumor volume was measured throughout the study

(day 0–10 and 17–23). On this schedule, 7.5 mg/kg resulted in 69% TGI. We next tested twice daily dosing in female mice bearing PA1 tumor xenografts (Table 1). On this schedule, 7.5 mg/kg was tolerated throughout the duration of the study and resulted in 78% TGI.

Anti-tumor activity of SCH 1473759 in combination with anti-mitotic agents

To follow up on the in vitro studies above, we evaluated the combination of SCH 1473759 with taxanes exploring several schedules. Mice bearing A2780 ovarian xenografts were treated with SCH 1473759 (100 mg/kg q7d), paclitaxel (20 mg/kg q7d) or the combination of both. These doses represent the maximally tolerated dose of these agents on a weekly schedule. Combinations explored included concurrent administration, paclitaxel 12 h before SCH 1473759, paclitaxel 4 h before SCH 1473759, and paclitaxel 4 h after SCH 1473759. Tumor growth inhibition was calculated at day 16, at which time vehicle-treated animals were sacrificed for humane reasons. Single agent SCH 1473759 and paclitaxel resulted in 52% ($P > 0.05$ vs. vehicle) and 35% ($P > 0.05$ vs. vehicle) TGI, respectively (Fig. 5b). Paclitaxel dosed 12 h before SCH 1473759 was the optimal schedule tested, resulting in 94% TGI ($P < 0.05$ vs. all groups). Paclitaxel administered concurrently, 4 h before SCH 1473759, and 4 h after SCH 1473759 resulted in 78, 86, and 80% TGI, respectively. Combination treatment with SCH 1473759 and paclitaxel was well-tolerated in all schedules in this study with only modest effects on body weight gain. Additionally, we found that SCH 1473759 enhanced the anti-tumor activity of a KSP inhibitor in A2780 tumor xenografts (data not shown).

We also evaluated a similar combination in 22RV-1 prostate tumor xenograft model. Single agent SCH 1473759 (100 mg/kg q7d) and docetaxel (15 mg/kg q7d) resulted in 68 and 61% TGI respectively ($P < 0.05$). The combination of docetaxel once a week followed 12 h later by SCH 1473759 resulted in enhanced TGI (84%, $P < 0.05$ vs. vehicle, $P > 0.05$ vs. single agents) although the benefits did not exceed statistical significance.

Discussion

SCH 1473759 was identified as a sub-nanomolar Aurora A/B inhibitor [16]. Here, we describe the biological activities of this compound. SCH 1473759 inhibited the phosphorylation of Histone H3, demonstrating potent on-target activity. Additionally, it potently induced >4 N DNA content, a phenotype consistent with Aurora B inhibition, at concentrations of the compound that resulted in inhibition of phosphorylation of Histone H3.

Several small molecule inhibitors have advanced to clinical trials. As these agents progress, it remains to be determined most sensitive patient populations, optimal dosing schedule, and best chemotherapeutic combinations. Using a panel of tumor cell lines and xenograft models, we sought to gain knowledge into each of these three areas.

We found that SCH 1473759 induced single-agent cell death across a panel of tumor cell lines from different tissue origins (myeloid, lymphoid, breast, ovarian, prostate, brain, skin, renal, gastric, lung, colon, and pancreas) and genetic backgrounds (p53, PTEN, etc.). The mean IC50 value for tumor growth inhibition across this panel was 21 nM. We did not find any particular tissue background or genetic trait as a driver of sensitivity or resistance. Further, similar activity was seen in cells that express varying levels of Aurora mRNA and in those that express the Aurora A SNP. The resistance of ASPC1 cells to SCH 1473759 appeared to be a unique property of this cell line because they were also found to be relatively resistant to MK-0457 (data not shown). Further studies on the mechanism of ASPC-1 resistance are warranted. These studies may provide important clues to acquired resistance or clinical insensitivity to Aurora inhibitors. Importantly, target engagement (induction of endoreduplication) and cell growth inhibition were seen in cell lines expressing PgP, including HCT-15 that overexpress PgP at high levels.

Similar to the findings in vitro for AT-9283 [17], we found that exposure times greater than 24 h to SCH

1473759 resulted in optimal cell growth inhibition and exposure times less than 24 h resulted in sub-optimal effects. This correlated with the finding that 24-h exposure was required for the induction of significant levels of >4 N DNA content. We found a similar requirement for MK-0457, AT-9283, and AZD-1152. Additionally, this time-dependence was seen in a larger panel of cell lines and most likely reflected the time it takes to complete cell doubling in an asynchronous population. These data with structurally unrelated compounds across multiple tumor cell lines suggests that Aurora inhibitors might be best used clinically on a dosing regime that would provide sufficient exposure to cover the entire tumor population doubling time.

Exposure time of 24 h SCH 1473759 was required to induce significant >4 N DNA content followed by 90% cell growth inhibition in asynchronous cells. A 16 h pre-treatment with taxanes or KSP inhibitor was sufficient to reduce the time required for the induction of cells with >4 N DNA content. Similar findings were observed with structurally unrelated Aurora A/B inhibitors (MK-0457 and AT-9283) and an Aurora B selective inhibitor (AZD-1152). For clinical application, our data suggest that shorter exposures to Aurora inhibitors may be sufficient when administered after taxane treatment. We found that SCH 1473759 accelerated the mitotic exit from taxane and KSP inhibitor arrest, establishing further rationale for these combinations.

To further explore the combination, we analyzed simultaneous treatment with SCH 1473759 and the anti-mitotic agents. In this situation, 4-h exposure to SCH 1473759 did not induce significant levels of >4 N DNA content; significant levels were only observed after a 24-h exposure. These data suggest that concurrent treatment with a taxane or KSP inhibitor is insufficient to reduce the exposure time required for an Aurora inhibitor to induce >4 N DNA content. This indicates that optimal therapeutic activity of the taxane or KSP inhibitor plus Aurora inhibitor combination will require appropriate sequencing in the clinical setting.

Inhibition of Aurora has been shown to override the spindle assembly checkpoint in paclitaxel- and monastrol- but not nocodazole-treated cells. Normally, this checkpoint ensures that anaphase does not occur until all kinetochores have attached to the spindle and there is equal tension from opposite poles. In paclitaxel- and monastrol-treated cells, the lack of proper tension goes undetected when Aurora is inhibited and cells exit mitosis prematurely [6, 18, 19]. This phenomenon was suggested to be driven by Aurora B inhibition [18]. Our findings are consistent with this proposed mechanism of Aurora B. SCH 1473759, MK-0457, AT-9283, and the Aurora B selective inhibitor AZD-1152 accelerated exit from taxane- and KSP inhibitor-induced arrest. Additionally, MLN8054 and Aurora A siRNA have also been reported to increase mitotic exit from paclitaxel- and nocodazole-induced arrest [20].

We demonstrated anti-tumor activity for SCH 1473759 in 4 human tumor xenograft models. Consistent with our findings in vitro and given the short half-life of SCH 1473759 in mice, continuous twice daily dosing was found to be superior to higher intermittent dosing. These data suggest dosing regimens that provide sufficient exposure to drug will be required for optimal activity in the clinic.

We found that SCH 1473759 enhanced the anti-tumor activity of taxanes *in vivo*. In these studies, combination treatment was well-tolerated with only modest effects on body weight gain. Previous studies have found that knockdown of Aurora A sensitizes cells to taxanes [21–23]. Further, others have demonstrated enhanced anti-tumor activity of Aurora inhibitors in combination with taxanes. However, dosing schedules used in these studies varied and only one study assessed scheduling sequences. Contrary to our work, SNS-314 on a biweekly schedule needed to be dosed first, followed 24 h later by docetaxel in order to show significant tumor growth inhibition [24]. On a biweekly schedule, docetaxel dosed first followed 24 h later by SNS-314 failed to result in any significant activity. Further, dosing of SNS-314 at its maximally tolerated dose was not tolerated in combination with docetaxel and dose reductions were required for combination studies.

Additionally, there are other reports of Aurora inhibitors in combination with taxanes, though optimal scheduling and sequencing were not explored. MK-0457 was shown to enhance docetaxel activity when MK-0457 was dosed twice daily for 2 days and docetaxel given on the second day [25]. The authors of this study suggested that differences in treatment schedule between MK-0457 and docetaxel was irrelevant, though data to support this notion was not presented. On the other hand, MK-5108 was found to enhance docetaxel activity when dosed twice daily for 2 days 24 h post-docetaxel [26]. AT-9283 showed enhanced efficacy with paclitaxel when paclitaxel was dosed weekly followed 24 h later with bid dosing of AT-9283 for 4 consecutive days [17]. Our findings demonstrate enhanced activity on all scheduling combinations tested, with the best efficacy observed when the taxane is dosed 12 h prior to SCH 1473759. This time point coincides with maximal induction of Histone H3 and MPM2 phosphorylation by taxanes and KSP inhibitors.

In conclusion, we have characterized a novel Aurora inhibitor. In vitro and in vivo, the compound demonstrates potent mechanism-based activity and activity was shown to be enhanced in combination with taxanes and KSP inhibitors. This information may be useful for optimizing the clinical efficacy of Aurora inhibitors.

Acknowledgments We would like to thank Drs. W.R. Bishop, R. Doll and M.A. Siddiqui for their advice and support. We thank Dr. Mohamed Ladha for his encouragement. We also thank Eugene Maxwell for his help, the entire Aurora team for their work and the Oncology in vivo dosing team, especially for the early morning and late night time points.

References

1. Mountzios G, Terpos E, Dimopoulos MA (2008) Aurora kinases as targets for cancer therapy. Cancer Treat Rev 34:175–182
2. Fu J, Bian M, Jiang Q, Zhang C (2007) Roles of Aurora kinases in mitosis and tumorigenesis. Mol Cancer Res 5:1–10
3. Andrews PD (2005) Aurora kinases: shining lights on the therapeutic horizon? Oncogene 24:5005–5015
4. Murnion ME, Adams RR, Callister DM, Allis CD, Earnshaw WC, Swedlow JR (2001) Chromatin-associated protein phosphatase 1 regulates aurora-B and histone H3 phosphorylation. J Biol Chem 276:26656–26665
5. Crosio C, Fimia GM, Loury R, Kimura M, Okano Y, Zhou H, Sen S, Allis CD, Sassone-Corsi P (2002) Mitotic phosphorylation of histone H3: spatio-temporal regulation by mammalian Aurora kinases. Mol Cell Biol 22:874–885
6. Morrow CJ, Tighe A, Johnson VL, Scott MI, Ditchfield C, Taylor SS (2005) Bub1 and aurora B cooperate to maintain BubR1-mediated inhibition of APC/CCdc20. J Cell Sci 118:3639–3652
7. Cimini D, Wan X, Hirel CB, Salmon ED (2006) Aurora kinase promotes turnover of kinetochore microtubules to reduce chromosome segregation errors. Curr Biol 16:1711–1718
8. Kimura M, Matsuda Y, Yoshioka T, Okano Y (1999) Cell cycle-dependent expression and centrosome localization of a third human aurora/Ipl1-related protein kinase, AIK3. J Biol Chem 274:7334–7340
9. Sasai K, Katayama H, Stenoien DL, Fujii S, Honda R, Kimura M, Okano Y, Tatsuka M, Suzuki F, Nigg EA, Earnshaw WC, Brinkley WR, Sen S (2004) Aurora-C kinase is a novel chromosomal passenger protein that can complement Aurora-B kinase function in mitotic cells. Cell Motil Cytoskeleton 59:249–263
10. Yang H, Burke T, Dempsey J, Diaz B, Collins E, Toth J, Beckmann R, Ye X (2005) Mitotic requirement for aurora A kinase is bypassed in the absence of aurora B kinase. FEBS Lett 579:3385–3391
11. Harrington EA, Bebbington D, Moore J, Rasmussen RK, Ajose-Adeogun AO, Nakayama T, Graham JA, Demur C, Hercend T, Diu-Hercend A, Su M, Golec JM, Miller KM (2004) VX-680, a potent and selective small-molecule inhibitor of the Aurora kinases, suppresses tumor growth in vivo. Nat Med 10:262–267
12. Howard S, Berdini V, Boulstridge JA, Carr MG, Cross DM, Curry J, Devine LA, Early TR, Fazal L, Gill AL, Heathcote M, Maman S, Matthews JE, McMenamin RL, Navarro EF, O'Brien MA, O'Reilly M, Rees DC, Reule M, Tisi D, Williams G, Vinković M, Wyatt PG (2009) Fragment-based discovery of the pyrazol-4-yl urea (AT9283), a multitargeted kinase inhibitor with potent aurora kinase activity. J Med Chem 52:379–388
13. Wilkinson RW, Odedra R, Heaton SP, Wedge SR, Keen NJ, Crafter C, Foster JR, Brady MC, Bigley A, Brown E, Byth KF, Barrass NC, Mundt KE, Foote KM, Heron NM, Jung FH, Mortlock AA, Boyle FT, Green S (2007) AZD1152, a selective inhibitor of Aurora B kinase, inhibits human tumor xenograft growth by inducing apoptosis. Clin Cancer Res 13:3682–3688
14. Manfredi MG, Ecsedy JA, Meetze KA, Balani SK, Burenkova O, Chen W, Galvin KM, Hoar KM, Huck JJ, LeRoy PJ, Ray ET, Sells TB, Stringer B, Stroud SG, Vos TJ, Weatherhead GS, Wysong DR, Zhang M, Bolen JB, Claiborne CF (2007) Antitumor activity of MLN8054, an orally active small-molecule inhibitor of Aurora A kinase. Proc Natl Acad Sci USA 104:4106–4111
15. Dar AA, Goff LW, Majid S, Berlin J, El-Rifai W (2010) Aurora kinase inhibitors - rising stars in cancer therapeutics? Mol Cancer Ther 9:268–278
16. Yu T, Tagat J, Kerekes A, Doll R, Zhang Y, Xiao Y, Esposite S, Belanger D, Curran P, Mandal A, Siddiqui A, Shih N, Basso A, Liu M, Gary K, Tevar S, Jones J, Lee S, Ponery S, Smith E, Hruza A, Voigt J, Ramanathan L, Prossie W, Hu M (2010). Discovery of SCH 1473759, a Novel Potent Injectable Inhibitor of Aurora Kinases based on the Imidazo-[1, 2,-a]-Pyrazine Core. ACS Med Chem Lett. doi:10.1021/R1100063w
17. Curry J, Angove H, Fazal L, Lyons J, Reule M, Thompson N, Wallis N (2009) Aurora B kinase inhibition in mitosis: strategies for optimising the use of aurora kinase inhibitors such as AT9283. Cell Cycle 8:1921–1929
18. Ditchfield C, Johnson VL, Tighe A, Ellston R, Haworth C, Johnson T, Mortlock A, Keen N, Taylor SS (2003) Aurora B couples chromosome alignment with anaphase by targeting BubR1, Mad2, and Cenp-E to kinetochores. J Cell Biol 161:267–280
19. Hauf S, Cole RW, LaTerra S, Zimmer C, Schnapp G, Walter R, Heckel A, van Meel J, Rieder CL, Peters JM (2003) The small molecule Hesperadin reveals a role for Aurora B in correcting kinetochore-microtubule attachment and in maintaining the spindle assembly checkpoint. J Cell Biol 161:281–294
20. Wysong DR, Chakravarty A, Hoar K, Ecsedy JA (2009) The inhibition of Aurora A abrogates the mitotic delay induced by microtubule perturbing agents. Cell Cycle 8:876–888
21. Tanaka E, Hashimoto Y, Ito T, Kondo K, Higashiyama M, Tsunoda S, Ortiz C, Sakai Y, Inazawa J, Shimada Y (2007) The suppression of aurora-A/STK15/BTAK expression enhances chemosensitivity to docetaxel in human esophageal squamous cell carcinoma. Clin Cancer Res 13:1331–1340
22. Hata T, Furukawa T, Sunamura M, Egawa S, Motoi F, Ohmura N, Marumoto T, Saya H, Horii A (2005) RNA interference targeting aurora kinase a suppresses tumor growth and enhances the taxane chemosensitivity in human pancreatic cancer cells. Cancer Res 65:2899–2905
23. Mazumdar A, Henderson YC, El-Naggar AK, Sen S, Clayman GL (2009) Aurora kinase A inhibition and paclitaxel as targeted combination therapy for head and neck squamous cell carcinoma. Head Neck 31:625–634
24. VanderPorten EC, Taverna P, Hogan JN, Ballinger MD, Flanagan WM, Fucini RV (2009) The Aurora kinase inhibitor SNS-314 shows broad therapeutic potential with chemotherapeutics and synergy with microtubule-targeted agents in a colon carcinoma model. Mol Cancer Ther 8:930–939
25. Lin YG, Immaneni A, Merritt WM, Mangala LS, Kim SW, Shahzad MM, Tsang YT, Armaiz-Pena GN, Lu C, Kamat AA, Han LY, Spannuth WA, Nick AM, Landen CN Jr, Wong KK, Gray MJ, Coleman RL, Bodurka DC, Brinkley WR, Sood AK (2008) Targeting aurora kinase with MK-0457 inhibits ovarian cancer growth. Clin Cancer Res 14:5437–5446
26. Shimomura T, Hasako S, Nakatsuru Y, Mita T, Ichikawa K, Kodera T, Sakai T, Nambu T, Miyamoto M, Takahashi I, Miki S, Kawanishi N, Ohkubo M, Kotani H, Iwasawa Y (2010) MK-5108, a highly selective Aurora-A kinase inhibitor, shows antitumor activity alone and in combination with docetaxel. Mol Cancer Ther 9:157–166